Lukas Michiels*

Marcus Geimer

Influence of High Pressure Drop Rates on Fatigue Crack Growth

Supporting Information available online

Hydraulic components in mobile machines are subjected to varying conditions and loads, which limit their lifetime. In particular, high pressure drop rates are suspected to increase fatigue crack growth rates. Existing studies on the fluid-structure interaction inside fatigue cracks during fast pressure drops do not explain increased crack growth in hydraulic systems. A laminar flow model was developed to simulate the fluid flow inside a crack under periodic pressure loads. The viscosity restrained the oil inside the crack, and the mechanical resistance of the closing crack led to a high pressure increase. Knowledge of the pressure profiles inside fatigue cracks helps to estimate the effective fatigue damage during transient loads.

1 Introduction

Use cases in mobile hydraulics are characterized by varying conditions and transient loads. Repeated loads above the fatigue limit lead to wear and eventually to failure of hydraulic components [1]. Even a few events above the fatigue limit can have a negative influence on the lifetime of a component through damage accumulation [2] and lead to failure if the damage aggregation reaches the fatigue limit [3]. Accurate prediction of fatigue damage is important for the design and testing of hydraulic components. Knowledge of the fatigue mechanism can eventually assist in real-time condition monitoring and damage accumulation. Nowadays, material fatigue tests are mostly performed in an accelerated process, in order to save time while assuming the damage to be independent of the load gradient. In hydraulic components, however, the damage does depend on the applied pressure gradient [4]. The action mechanism of the component itself or external loads can cause pressure gradients. For example, the piston chamber of an axial piston pump with a compression angle of 12° undergoes a pressure gradient of 10^6 bar s^{-1} for a pressure rise from 0 to 250 bar at a pump speed of 7800 rpm [5]. These pressure gradients occur both as positive and negative gradients. The impact of a wheel loader's bucket during loading is an example of external loads causing high pressure gradients. The resulting gradient can exceed a rate of 2×10^4 bar s^{-1} [6] and represents an extraordinary stress for all connected components.

Certain standards have been established for pressure impulse tests. Hoses are tested by periodic pressure loads in compliance with ISO 6802 and ISO 6803. A typical cycle consists of a pressure rise before the nominal pressure is held for a certain period and then reduced to the lower pressure level. The gradients are defined by the test frequency (0.5–1.3 Hz) and the nominal (system) pressure. For high-pressure components, the pressure

rise gradients are in the range of $(2.5–6.5) \times 10^4$ bar s^{-1}, which is up to 100 times lower than the gradients occurring in mobile machines. Similar standards have been established for active and passive components in hydraulic systems in the aerospace sector (ISO 6772:2012). In contrast to the positive pressure gradient, the pressure drop rate is not specified in these regulations.

Studies on the effect of fluid-material contact are known from related fields. Davis and Ellison studied the effect of hydrodynamic pressure on crack propagation in submerged specimens [7]. Their experiments showed that the fluid viscosity opposed the closing of the crack and that the stress amplitude was reduced due to an increased lower stress level of the crack, leading to a small decrease in the crack propagation rate. Lower crack propagation rates for highly viscous fluids have also been reported [8], and the effect of high ambient pressure on fatigue crack growth has been studied [9]. Crack grow rates at cycle frequencies of 1 and 5 Hz at high oil pressure were studied, with lower crack grow rates for higher frequency loads, while crack grow rates were generally increased by high ambient pressure [9]. Tzou et al. [10] reported an increase in crack growth rates for low fatigue levels, while at high fatigue levels oil has a reducing effect on crack growth rates. In contrast to hydraulic components, in which the material stress and deformation of the component are caused by the fluid, in these experiments, the specimens were submerged in the fluid and an external load was applied. Flow regimes in cracks come to attention with the concept of "leak before break" (LBB). While

Lukas Michiels, Prof. Dr.-Ing. Marcus Geimer
lukas.michiels@kit.edu
Karlsruhe Institute of Technology, Institute of Mobile Machines (Mobima), Rintheimer Queralle 2, 76131 Karlsruhe, Germany.

Wiley Online Library

the majority of research has focused on large cracks with applications in the power industry, some work has been done on narrow cracks, such as those found in pressurized gas cylinders [11–13]. A model of laminar flow performed well for cracks when the grain size is smaller than the crack width, while for small crack widths, modeling the turns and bends due to material roughness is more accurate [11]. Bagshaw et al. used a simplified computational fluid dynamics (CFD) model to simulate flow rates in narrow cracks smaller than three times the magnitude of the surface roughness [12].

Another related topic is fatigue crack propagation in lubricated components with surface contact pressure. Crack propagation has been investigated in driven over-rail systems [4, 14–17]. Bower stated that cracks in railway tracks occur, especially when there is a fluid on the rails [4]. Crack growth of an existing crack only occurred at an angle similar to the direction of movement and when the course of the crack also pointed in the direction of movement. Otherwise, the crack stagnated. In these cases, fluid is pressed into the crack by the external load of the wheel, which results in a hydrostatic pressure and a wedge effect inside the crack. The theory of the underlying models and the investigations in [18] point out that mixed stress intensity factors of mode I (opening) and modes II and III (shear) act at the crack tip due to their individual effects. Modes II and III occur primarily due to the mechanical loading of the rail crossing, which can be neglected for the approach presented in this paper.

Current research focuses on crack propagation in hydraulic fracture systems, e.g., in oil and gas wells [19–21]. The main considerations are the flow of a viscous fluid in an existing crack, the crack propagation due to the hydraulic pressure, and the deformation due to internal and external loads. Other publications in this field focused on modeling these effects with the extended finite element method (XFEM) [22–24]. High rates of pressure change during cyclic loads and possible correlated effects, e.g., the oil wedging postulated by research on crack propagation of railway tracks, were not part of these studies. The methods used to model material fatigue could potentially be adapted to crack growth in hydraulic components.

The above-mentioned studies lead to inclusive results on the effect of fluid on material fatigue and its influence on component lifetime. The influence of the pressure drop rate on the fatigue crack growth of hydraulic components is yet to be identified. The aim of this paper is to describe the fluid flow and the pressure levels inside a crack for high pressure drop rates and to quantify their influence on fatigue crack growth. A laminar flow model was developed for this purpose. The high-pressure interior of an axial piston pump inspired the studied geometry, which was proposed in [25], with an already estab-
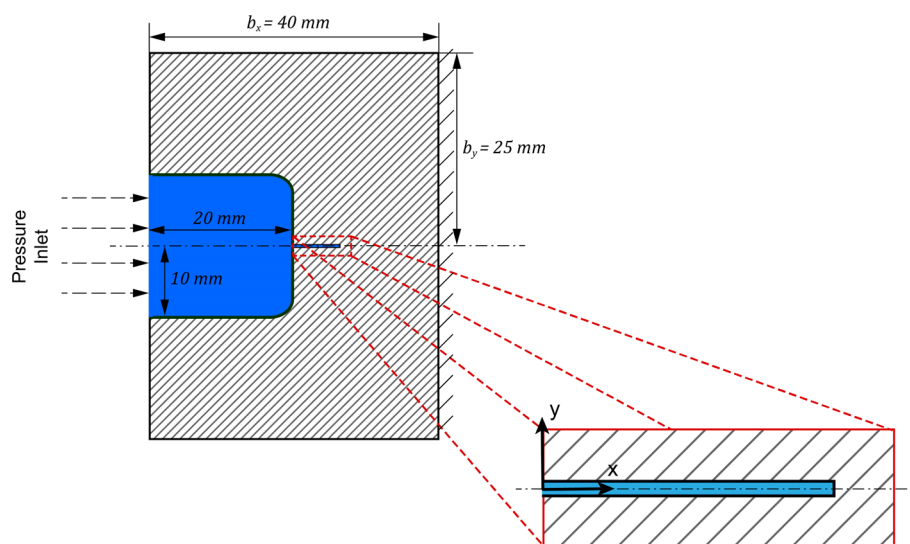

Figure 1. Geometry of the studied part with the fluid domains in blue (pressure chamber: dark blue, crack: light blue), the fixed support on the right, and the pressure inlet on the left.

lished fatigue crack. Fig. 1 shows a 2D representation of the studied geometry, in which the crack was centered on the opposite face of the pressure inlet at a straight angle. Through the pressure inlet on the left side of the geometry, the external pressure load was applied.

First, the elastic deformation of the component was studied under the influence of pressurized fluid inside the crack to quantify the wedging effect of trapped fluid. Then, a laminar flow model was added to account for the fluid flow during crack closure, and a parameter study was performed to quantify the effect of different pressure levels and pressure drop rates. Finally, linear elastic stress intensity factors were used to determine the crack growth rates for the simulated load profiles.

2 Linear Elastic Crack Deformation

2.1 Elastic Crack Opening Displacement

The elastic deformation of the solid causes the crack gap to open when the load pressure is applied (pressure rise) and close (pressure drop) when the load pressure is released. During one load cycle, the load pressure is applied with a certain positive pressure rise rate, held for a certain time, and released with a certain negative pressure drop rate. The elastic deformation of the crack region, as shown in Fig. 1, is simulated with the commercial finite element method (FEM) solver Ansys in a 3D simulation. The mesh consists of a single layer and symmetry conditions in the third direction, resulting in a pseudo-2D simulation. The solid regions are meshed with hexahedron and prism elements with linear basis functions. Around the crack and the crack tip, the mesh is refined by factors of 10 and 100, leading to a total of 14,750 elements for the solid part. The fluid pressure is assumed to be identical at all regions (Fig. 1) and equal to the nominal load pressure before the pressure drop. The material of the loaded part is modeled with linear elastic

material behavior and a Young's modulus of $E^{1)}$ = 210 GPa and a Poisson's ratio of ν = 0.3. The oil is assumed to be an incompressible Newtonian fluid with the characteristics described in Sect. 3.1. The deformation of the crack region was assumed to be small compared to the dimensions of the part, and linear, purely elastic deformation normal to the crack faces was assumed. Under the assumption of linear deformation, the crack opening displacement ε_y in Eq. (1) can be expressed as a superposition of the crack opening displacement of a deformed piece $\varepsilon_{y,e}$ caused by the pressure force (of the fluid) on the component faces (external pressure field) and the additional deformation $\varepsilon_{y,i}$ caused by the fluid pressure on the crack faces (internal pressure field).

$$\varepsilon_y(x) = \varepsilon_{y,i}(x) + \varepsilon_{y,e}(x) \tag{1}$$

The crack opening displacements caused by the internal and external pressure are simulated separately by applying the load pressure solely to the pressure chamber or to the crack faces. For linear-elastic materials, the deformations can be superposed to calculate the total linear-elastic deformation.

During a pressure drop, the oil has to flow out of the crack for the crack tip opening displacement to become zero (crack closure). A rising pressure gradient from the crack mouth to the crack tip is established as the oil flows out of the crack. The maximum pressure of the oil is limited by the material resistance. The oil pressure is equal to the force required for a crack deformation of the size of the current oil volume. This leads to an equilibrium between the flow resistance of the oil and the material resistance of the solid part. First, a pressure release with a nearly infinite pressure drop rate is theoretically considered. The release time Δt is the ratio of the system pressure p_0 and the drop rate Δp_0. As p_0 is a constant and $\Delta p_0 \Delta \rightarrow \infty$, $\Delta t = p_0 / \Delta p_0 \rightarrow 0$, the strain rate of a Newtonian fluid $\tau = \eta(\mathrm{d}u/\mathrm{d}y) \rightarrow \infty$, in which η is the dynamic viscosity and u the velocity, as well as the hydrodynamic pressure $\Delta p_{\mathrm{dyn}} \rightarrow \infty$. Hence, Δp_{dyn} is considerably greater than the elastic resistance of the material. In this case, the oil flow during the pressure drop can be neglected. Without oil flow, the total deformation is constant during the pressure drop. The deformation caused by the force of the external pressure field is, however, decreasing.

The normal pressure $\sigma_y(x)$ required for the crack to remain open is simulated by imposing the crack opening deformation $\varepsilon_y(x,p_0)$ as a boundary condition. The normal pressure $\sigma_y(x)$ required for the crack to remain completely open is, in theory, the highest possible oil pressure in the case of high pressure drop rates.

Under the assumption of linear elastic strain, the strain-pressure ratio $\varepsilon_y(x,p_0)/p_0$ is constant, and the overpressure factor k_{p}, defined in Eq. (2), is introduced. The overpressure factor only depends on the geometry of the component and material properties and is independent of the system pressure.

$$k_{\mathrm{p}}(x) = \frac{\sigma_y(x,p_0)}{p_0} \tag{2}$$

The crack opening displacement is considerably larger at the crack mouth than towards the crack tip. In consequence, the relative volume change during crack closure has its peak at the crack mouth. The linear elastic resistance, however, does vary considerably less over the length of the crack. Fig. 2 shows overpressure factors for the studied component. It varies along the crack length. The highest crack overpressure factor is observed at the crack mouth, and it decreases towards the crack tip. Under certain conditions, this variation could result in oil being pressed into the crack. An oil flow towards the crack tip would lead to increased deformation of the crack tip region. However, the crack tip deformation does not solely depend on the crack tip pressure, but also on the complete crack pressure profile and deformation. Hence, the complete pressure profile during the pressure drop inside the crack must be studied, and a specific crack tip pressure alone does not allow the conclusion of an increased crack tip deformation. At the crack tip, the overpressure factor is equal to one, as the stress intensity has a singularity at the crack tip for linear elastic models [26].
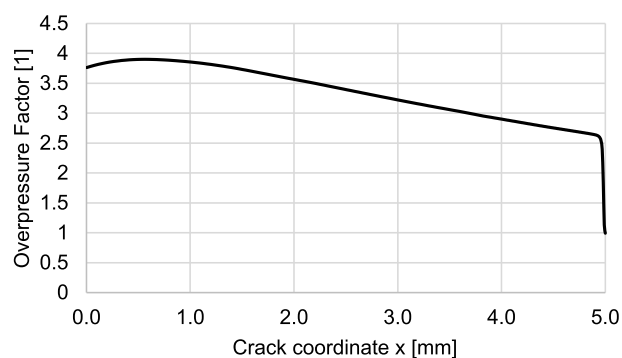

Figure 2. Overpressure factor for a component width of b_y = 25 mm.

3 Crack Flow Regime

For typical pressure drop rates, the oil flow cannot be neglected during pressure release. A simplified model is introduced in the following to account for the fluid flow inside the crack.

3.1 Laminar Fluid Flow

Fluid flow rates through cracks have been analyzed and compared to theoretical results when assuming laminar flow between two parallel planes or flow through a pipe with bends and changes in area [11]. The assumption of a laminar flow between two parallel planes is accurate for large crack widths. However, it underestimates the fluid flow through small cracks with crack openings equal to or smaller than the surface roughness. In the following, laminar flow is assumed for all crack dimensions, as the introduced errors are assumed to be small. Additionally, the flow resistance is proportional to the pressure drop rate. Therefore, an over- or underestimation of the flow resistance would lead to an over- or underestimation of the corresponding pressure drop rates, but not alter the theoretical

---

1) List of symbols at the end of the paper.

considerations. The oil is considered to be a non-compressible Newtonian fluid with a dynamic viscosity of $\eta = 0.046\,\mathrm{Pa\,s}$ and a density of $\rho = 860\,\mathrm{kg\,m^{-3}}$.

For two parallel planes which extend to a great length, the volume flow Q in Eq. (3) can be calculated as a function of the pressure drop Δp, the planes' geometry b, h, and l, and the dynamic viscosity η of the fluid [27].

$$Q = \frac{bh^3}{12\eta l}\Delta p \tag{3}$$

For cracks in hydraulic components, the assumption of a constant height is not valid. The cross section of the crack decreases from the crack mouth to the crack tip. However, the change in the cross section of up to $50\,\mu\mathrm{m}$ is assumed to be small compared to the length of the crack. The crack was modeled as M discrete sections with constant height. In the case of a pressure drop, the crack opening displacement is time-dependent. Eq. (4) calculates the fluid flow Q between two discrete time steps $\Delta t = t_\mathrm{n} - t_{\mathrm{n}-1}$ based on the crack size difference $\Delta h(x)$, the crack width b, and the section length Δl.

$$\Delta Q(x) = \frac{\Delta l\, b\, \Delta h(x)}{\Delta t} \tag{4}$$

Eqs. (3) and (4) can be used to derive the fluid pressure loss for a crack section during crack closure in Eq. (5) and the total fluid pressure at position $x = x_\mathrm{m}$, $m \in [1,M]$ and time t_n, $t \in [1,N]$ by using the cumulative sum and the load pressure $p_0(t_\mathrm{n})$ in Eq. (6).

$$\Delta p(x_\mathrm{m}, t_\mathrm{n}) = \frac{12\,\eta\Delta l\,\int_{x_\mathrm{m}}^{l_0}\Delta h(\hat{x}, t_\mathrm{n})\mathrm{d}\hat{x}}{h(x_\mathrm{m}, t_\mathrm{n})^3\Delta t} \tag{5}$$

$$p(x_\mathrm{m}, t_\mathrm{n}) = p_0(t_\mathrm{n}) + \sum_{\hat{m}=0}^{m}\Delta p(x_{\hat{m}}, t_\mathrm{n}) \tag{6}$$

Eq. (6) is used to calculate the hydrodynamic pressure when assuming that the crack is closed after pressure release for a given system pressure and a specific pressure drop rate. The results for certain system pressure levels and pressure drop rates are plotted in Fig. 3. Given the magnitude of the dynamic pressure at higher drop rates, it must be assumed that the majority of the oil is not flowing out of the crack during the pressure release but is forcing the crack to remain open.

Coupling the laminar flow model with the finite element simulation would increase the computational cost considerably. A linear elastic approximation is used in combination with a polynomic regression to limit computational costs. Each discrete section $x = x_\mathrm{m}$, $m \in [1,M]$ has a constant height. Eq. (7) calculates the crack size, which consists of the internal $h_\mathrm{i}(x,t_\mathrm{n})$ and external $h_\mathrm{e}(x,t_\mathrm{n})$ pressure field, in relation to the current pressure $p(x,t_\mathrm{n})$ in this section, the reference pressure p_ref, and the coefficients $a_0 \ldots a_\mathrm{n}$. The elastic interdependency between
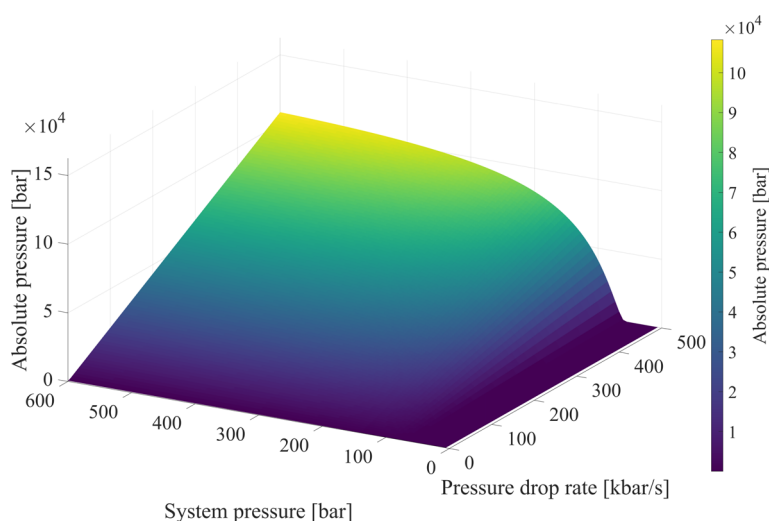

Figure 3. Absolute pressure for different system pressures and pressure drop rates under the assumption of complete crack closure during pressure drop.

the discrete sections of a constant crack height is neglected. The total crack opening displacement $h(x,t_\mathrm{n})$ is the sum of the displacement caused by the external load pressure $h_\mathrm{e}(x,t_\mathrm{n})$, the pressure inside the crack acting on the crack faces $h_\mathrm{i}(x,t_\mathrm{n})$, and the initial crack size of the unloaded crack in correspondence to the FEM model.

$$h(x, t_\mathrm{n}) = h_\mathrm{i}(x, t_\mathrm{n}) + h_\mathrm{e} + h_0$$

$$\text{with } h_\mathrm{i}(x, t_\mathrm{n}) = \frac{p(x, t_\mathrm{n})}{p_\mathrm{ref}}\left(a_0 + a_1 x + \ldots + a_\mathrm{n}x^l\right) \tag{7}$$

$$\text{and } h_\mathrm{e}(x, t_\mathrm{n}) = \frac{p_0(t_\mathrm{n})}{p_\mathrm{ref}}\left(a_0 + a_1 x + \ldots + a_\mathrm{n}x^l\right)$$

Neglecting the elastic interdependency between the discrete sections leads to an underestimation of the crack size at the crack mouth ($x < 1\,\mathrm{mm}$). The pressure at the crack mouth is close to zero after the release of the system pressure. The deformation of the crack mouth is, however, not zero and depends on the other parts of the deformed crack. The crack size approximation is extended with the condition that the crack size cannot diminish for $x \to 0$ to account for this interdependency. A more accurate approximation is possible when considering the effect of every section and modeling the crack heights as matrix operation $\overline{h_\mathrm{i}}(x, t_\mathrm{n}) = \mathbf{A}\bar{p}(t)$ with the square matrix $\mathbf{A} = [a_{\mathrm{i,j}}]$. Each coefficient $a_{\mathrm{i,j}}; i,j \in [0,m]$ describes the influence of the pressure at section j on the crack opening displacement at section i. Obtaining the coefficients $a_{\mathrm{i,j}}$ of the matrix $\mathbf{A}$, however, is not trivial, as $\mathbf{A}$ has m^2 unknown coefficients, whereas $\overline{h_\mathrm{i}}(x, t_\mathrm{n}) = \mathbf{A}\bar{p}(t_\mathrm{n})$ are only m equations. Thus, m independent pressure profiles $\bar{p}(t_\mathrm{n})$ are required to calculate A.

The laminar flow equations cannot be solved directly, as $h(x, t_\mathrm{n})$ and $p(x, t_\mathrm{n})$ are unknown. The load pressure $p_0(t_\mathrm{n})$ is used as a boundary condition and as the initial solution for all $p(x, t_\mathrm{n})$. Using Eqs. (6) and (7), the system is iterated towards its steady state (Fig. 4). When using a high temporal resolution, small changes in the crack size $h(x, t_\mathrm{n})$ lead to
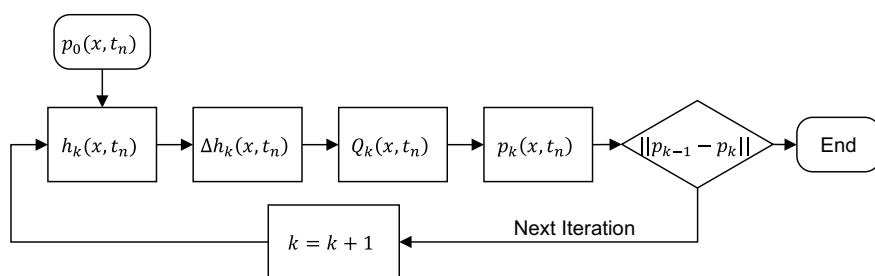
Figure 4. Laminar fluid simulation flow chart.

considerable pressure peaks and the system has difficulties converging. For this reason, a high relaxation factor of $\alpha \in [0.9, \ 0.99]$ is used to stabilize the pressure variable

$$p_{\mathrm{k}}(x, t_n) = \alpha p_{k-1}(x, t_n) + (1 - \alpha)\tilde{p}_{\mathrm{k}}(x, t_n). \tag{8}$$

The laminar flow approximation is compared to the solution of the finite element solver for validation (see Supporting Information).

3.2 Influence of Load Parameters

In the following it is assumed that the crack is filled with pressurized oil. Raise rate and hold time influence the fluid pressure inside the oil (see Supporting Information).

3.2.1 System Pressure

The maximum system pressure influences the crack pressure in two ways. Under the assumption of linear elastic deformation, the system pressure is proportional to the deformation and, as a consequence, to the crack size (Eq. (7)). If the crack size is increased, the internal crack pressure required to maintain the total deformation also increases proportionally. On the other hand, the flow resistance decreases cubically with increasing crack size (Eq. (3)). As a consequence, the relative pressure overshoot decreases with increasing system pressure. For low system pressure, no pressure overshoot can be identified, which can be explained by the initial crack size. If the initial crack size is similar to the total deformation, or even larger, the pressure overshoot becomes insignificant. As the assumption of a certain size of an initial crack is a consequence of the meshing of the fluid domain in finite volume simulations, it is considered a modeling error. Since very low system pressures do not pose a challenge regarding material fatigue, very low system pressures are neglected in this paper.

Fig. 5 shows the pressure overshoot for different pressure levels applied to the same geometry. While the absolute pressure increases for higher system pressures, the relative overpressure factor has its peak at 125 bar and decreases with the system pressure. The pressure overshoot reaches its maximum at 900 bar. For a system pressure above 900 bar, the overpressure factor of 1 indicates that the internal crack pressure does not exceed the system pressure and no overpressure inside the crack occurs.

3.2.2 Viscosity and Pressure Drop Rate

The laminar flow property (Eq. (3)) gives a proportional ratio between the flow rate Q and the dynamic viscosity η The volume flow rate is proportional to the crack size (Eq. (4)), which depends on the pressure drop rate. From the theoretical background, it can be concluded that the viscosity and the drop rate are proportional and reducing the viscosity has the same effect as reducing the pressure drop rate.

In a certain range, the maximal overpressure increases for higher pressure drop rates. However, the pressure overshoot is bound, as it does not exceed the theoretical maximum derived in Sect. 2 and does correspond to the system pressure for low drop rates. Fig. 6 shows the maximum crack pressure in relation to the pressure drop rate. The maximum fluid pressure inside the crack, which is observed at the crack tip, exceeds the elastic pressure of the material for a constant deformation. This leads to the theory that the non-uniform pressure distribution, provoked by the fast release of the system pressure, leads to oil being pushed into the crack tip. An increased deformation at the crack tip region could then cause increased fatigue damage.
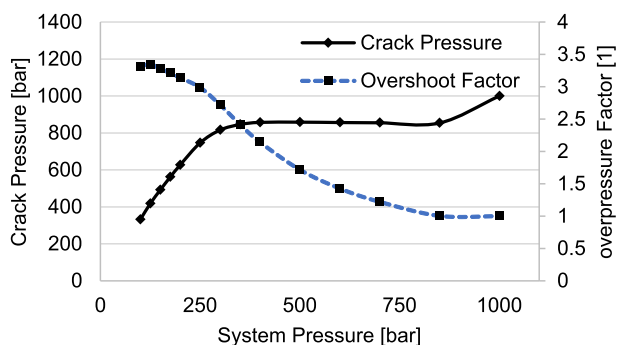

Figure 5. Maximum crack pressure and overpressure factor for a pressure drop rate of 500 kbar s^{-1} and various system pressures.
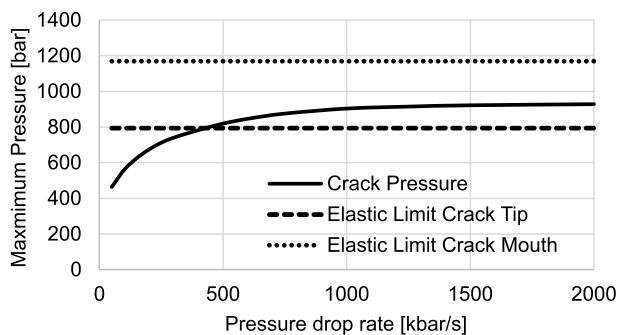

Figure 6. Maximum crack pressure compared to theoretical elastic pressure for a constant crack deformation (system pressure = 300 bar)

4 Fatigue Crack Propagation

Linear elastic stress intensity factors describe the effective fatigue damage of linear elastic stress and strain in the vicinity of a crack. For mode 1 loads, the stress intensity factor K_I can be calculated by using the crack strain occurring on the crack faces v_{FEM} (Eq. (8)) [28]. As the component is studied as a 2D piece, the plane strain state is assumed.

$$K_I = \lim_{r \to \infty} \frac{E}{(4-v)(1+v)} \sqrt{\frac{2\pi}{r}} v_{FEM} \qquad (9)$$

Following the results of the laminar approximation of Sect. 3.2.2, the load case of a system pressure of 300 bar and a pressure drop rate of 100 kbar s^{-1} was used. For a crack pressure above 800 bar the deformation at the crack tip could be increased compared to the nominal load. Similar to the approach in Sect. 3.1, the resulting pressure sequence of the laminar flow model was used as a boundary condition for the FEM simulation. Fig. 7 shows the used pressure sequence, the maximum crack tip pressure, and the stress intensity factors during one load cycle. The fluid pressure at the crack tip does exceed the theoretical limit of 800 bar.
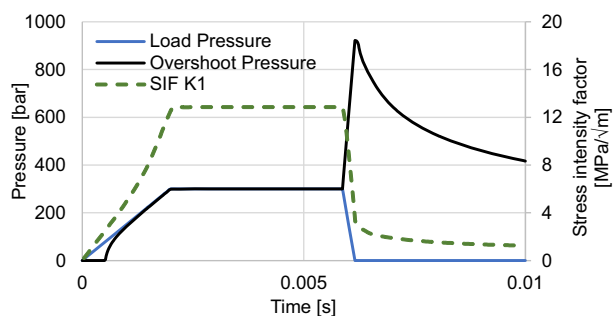
Figure 7. Stress intensity factor and pressure sequence during one load cycle for a system pressure of 300 bar and a pressure drop rate of 1,000 bar s^{-1} (solid) and mode 1 stress intensity factor (SIF K1, dashed).

The crack size simulated with the FEM solver showed no increase in the crack tip's deformation during pressure release. Fig. 8 shows the crack size and the linear elastic stress intensity factors under nominal load and at the time of the maximum crack pressure. Due to the high pressure overshoot, the crack tip and the crack opening did not close at the same rate. The influence of the local pressure at the crack tip was not sufficient to cause the crack tip deformation to increase. Even with a pressure overshoot of this magnitude, no oil was flowing into the crack tip. The linear elastic stress intensity factors, which depend after Eq. (9) solely on the elastic strain, did not increase either. This leads to two possible conclusions, either the pressure overshoot is not increasing fatigue damage, or the linear elastic stress intensity factors are not able to explain the additional fatigue damage.

Currently, there are two explanations for the absence of increased fatigue damage. First, elastic deformation is not suffi-
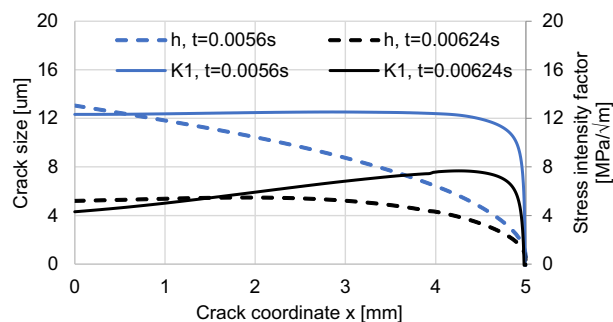
Figure 8. Stress intensity factor approximation according to FEM crack face displacement at two time steps (t = 0.056 s, nominal pressure; t = 0.00624 s, maximum crack overshoot pressure).

cient to explain the ongoing mechanism inside the crack. A possible hypothesis would be that the increased internal pressure leads to an increase in the plastic zone around the crack tip and, as a consequence, to faster crack growth. Second, impulse tests are sometimes performed at frequencies that lead to partially filled cracks, where an increase in crack tip strain for high pressure drop rate occurs (see Supporting Information). This seems unlikely, as the overall crack growth rate should be lower than in the case of low cycle frequencies with a long hold time when the internal crack field is established.

5 Conclusion

The fluid-structure interaction inside a fatigue crack filled with oil inside a hydraulic component was studied, and the flow regime during pressure drop was modeled. In the case of high pressure drop rates, the oil does not flow out of the crack during the pressure drop due to the flow resistance of the oil, and the fluid pressure inside the crack increases. In a theoretical consideration, infinite drop rates were used to simulate the linear elastic pressure limit. In this case, the crack opening deformation is constant and the magnitude of the strain caused by the internal crack pressure field and external load pressure is used to introduce a new load-independent overpressure factor. Overpressure factors can be used to compare different geometries and to describe how the elastic material resistance influences the resulting pressure magnitude. Especially in the front part of the crack, the fluid pressure must increase considerably to cause the required deformation for the crack to remain open.

A laminar model was used to account for the fluid flow and was combined with the FEM results. To decrease computational costs, the elastic resistance of the component was simplified and modeled as a polynomial regression. The simulation supports the assumption of increased pressure inside the crack during the pressure release and shows the influence of pressure drop rate, viscosity, and system pressure. In the case of partially filled cracks, oil flow into the crack tip can be observed. For completely filled cracks, however, no flow into the crack tip is observed, and the crack tip deformation does not increase during pressure drop. As a consequence, the resulting fatigue

damage, which solely depends on the elastic strain, does not support the hypothesis of increased crack growth for high pressure drop rates.

In future work, CFD should be used to validate the findings of the laminar flow model. The CFD solver can be directly coupled to the FEM solver to account for the fluid-structure interaction and to avoid discrepancies in the deformation of the crack faces caused by the polynomial regression. In a second step, XFEM could be adapted to simulate crack growth. Additionally, plastic deformation can be included in the mechanic analyses to take non-linear and material hardening effects into account. In particular, the influence of the pressure on the size of the plastic zone should be the subject of future studies, since an increased plastic zone would result in altered fatigue crack growth.

Supporting Information

Supporting Information for this article can be found under DOI: https://doi.org/10.1002/ceat.202200385. This section includes additional references to primary literature relevant for this research [XX–XY].

Acknowledgment

The authors have declared no conflict of interest.

Symbols used

a	[–]	coefficient
$\mathbf{A}$	[–]	matrix
b	[mm]	crack width
b_x	[mm]	component size (x)
b_y	[mm]	component size (y)
E	[MPa]	Young's modulus
h	[µm]	total crack size
h_0	[µm]	initial crack size
h_i	[µm]	crack opening displacement by internal pressure load
h_e	[µm]	crack opening displacement by external pressure load
k_p	[–]	overpressure factor
K_I	[MPa m$^{-1/2}$]	mode 1 stress intensity factor
l	[m]	crack length
M	[–]	number of sections
p	[bar]	absolute fluid pressure
p_0	[bar]	nominal (system) pressure
p_{ref}	[bar]	reference pressure
Δp_0	[bar s^{-1}]	pressure drop rate
Δp_{dyn}	[bar]	hydrodynamic pressure
Q	[m^3]	volume flow
t	[s]	time
u	[m s^{-1}]	velocity
x	[mm]	crack coordinate

Greek letters

α	[–]	relaxation factor
ε_y	[µm]	total elastic crack deformation
$\varepsilon_{y,i}$	[µm]	elastic crack deformation by internal pressure field
$\varepsilon_{y,e}$	[µm]	elastic crack deformation by external pressure field
η	[Pa s]	dynamic viscosity
ρ	[kg m^{-3}]	fluid density
ν	[–]	Poisson's ratio
ν_{FEM}	[m]	crack face displacement
σ_y	[MPa]	normal pressure on crack faces
τ	[s^{-1}]	strain rate

Abbreviations

CFD	computational fluid dynamics
FEM	finite element method
SIF	stress intensity factor
XFEM	extended finite element method

References

[1] *Hydraulic Failure Analysis: Fluids, Components, and System Effects* (Eds: G. Totten, D. Wills, D. Feldmann), ASTM International, West Conshohocken, PA **2001**.

[2] S. K. Paul, S. Tarafder, *Int. J. Pressure Vessels Piping* **2013**, *101*, 81–90.

[3] M. Boog, *Ph.D. Thesis*, Karlsruhe Institute of Technology **2011**.

[4] A. F. Bower, *J. Tribology* **1988**, *110*, 704–711.

[5] S. Jian, L. Xin, W. Shaoping, *Math. Probl. Eng.* **2014**, *2014*, 1–10.

[6] L. Brinkschulte, *Ph.D. Thesis,* Karlsruhe Institute of Technology **2021**.

[7] F. H. Davis, E. G. Ellison, *Fatigue Fract. Eng. Mater. Struct.* **1989**, *12*, 527–542.

[8] C. J. Polk, W. R. Murphy, C. N. Rowe, *A S L E Trans.* **1975**, *18*, 290–298.

[9] W. J. Plumbridge, P. J. Ross, J. S. C. Parry, *Mater. Sci. Eng.* **1985**, *68*, 219–232.

[10] J. L. Tzou, S. Suresh, R. O. Ritchie, in *Mechanical Behaviour of Materials* (Eds: J. Carlsson, N. G. Ohlson), Pergamon, **1984**, 711–717.

[11] L. V. Clarke, H. Bainbridge, S. B. M. Beck, J. R. Yates, *Int. J. Pressure Vessels Piping* **1997**, *71*, 71–75.

[12] N. M. Bagshaw, S. B. M. Beck, J. R. Yates, *Proc. Instit. Mech. Eng., Part C: J. Mech. Eng. Sci.* **2000**, *214*, 1099–1106.

[13] C. Hong, Y. Asako, J.-H. Lee, *J. Pressure Vessel Technol.* **2009**, *131*. DOI: https://doi.org/10.1115/1.3147984

[14] P. E. Bold, M. W. Brown, R. J. Allen, *Wear* **1991**, *144*, 307–317.

[15] M. Akama, T. Mori, *Q. Rep. RTRI* **2005**, *46*, 231–237.

[16] D. I. Fletcher, P. Hyde, A. Kapoor, *Proc. Instit. Mech. Eng., Part F: J. Rail Rapid Transit* **2007**, *221*, 35–44.

[17] D. I. Fletcher, P. Hyde, A. Kapoor, *Wear* **2008**, *265*, 1317–1324.

[18] P. E. Bold, M. W. Brown, R. J. Allen, *Fatigue Fract. Eng. Mater. Struct.* **1992**, *15*, 965–977.

[19] Z.-K. Hou, H.-L. Cheng, S.-W. Sun, J. Chen, D.-Q. Qi, Z.-B. Liu, *Appl. Geophys.* **2019**, *16*, 243–251.

[20] Y. Cheng, Y. Lu, Z. Ge, L. Cheng, J. Zheng, W. Zhang, *Fuel* **2018**, *218*, 316–324.

[21] Y. Zhao, S. Cao, D. Shang, H. Yang, Y. Yu, Y. Li, J. Liu, H. Wang, R. Pan, H. Yang, B. Zhang, H. Tu, *Comput. Geotech.* **2019**, *111*, 229–242.

[22] E. Gordeliy, A. Peirce, *Comput. Methods Appl. Mech. Eng.* **2013**, *253*, 305–322.

[23] H. Wang, *J. Pet. Sci. Eng.* **2015**, *135*, 127–140.

[24] N. Weber, *Ph.D. Thesis*, RWTH Aachen University **2016**.

[25] J. Happel, *Master's Thesis*, Karlsruhe Institute of Technology **2018**.

[26] D. Gross, T. Seelig, *Bruchmechanik*, Springer Vieweg, Berlin **2011**.

[27] B. S. Massey, *Mechanics of Fluids*, Van Nostrand Reinhold, **1989**.

[28] H. A. Richard, M. Sander, *Ermüdungsrisse: erkennen, sicher beurteilen, vermeiden*, Vieweg + Teubner, Wiesbaden **2009**.